Nonlinear Identifiability Analysis of the Porous Electrode Theory Model of Lithium-Ion Batteries

Journal of The Electrochemical Society, 2021 **168** 090546

Nonlinear Identifiability Analysis of the Porous Electrode Theory Model of Lithium-Ion Batteries

Marc D. Berliner,[1,z] Hongbo Zhao,[1] Supratim Das,[1] Michael Forsuelo,[1] Benben Jiang,[1] William H. Chueh,[2,3] Martin Z. Bazant,[1] and Richard D. Braatz[1]

[1]*Massachusetts Institute of Technology, Cambridge, Massachusetts 02139, United States of America*
[2]*SLAC National Accelerator Laboratory, Menlo Park, California 94025, United States of America*
[3]*Stanford University, Stanford, California 94305, United States of America*

Porous electrode theory (PET) is widely used to model battery cycling behavior by describing electrochemical kinetics and transport in solid particles and electrolyte, and modeling thermodynamics by fitting an open-circuit potential. The PET model consists of tightly coupled nonlinear partial differential-algebraic equations in which effective kinetic and transport parameters are fit to battery cycling data, and then the model is used to analyze the effects of variations in design parameters or operating conditions such as charging protocols. In a detailed nonlinear identifiability analysis, we show that most of the effective model parameters in porous electrode theory are not practically identifiable from cycling data for a lithium-ion battery. The only identifiable parameter that can be identified from C/10 discharge data is the effective solid diffusion coefficient, indicating that this battery is in the diffusion-limited regime at this discharge rate. A resistance in series correlation was shown for the practically unidentifiable parameters by mapping out the confidence region. Alternative experiments in addition to discharge cycles are required in order to uniquely determine the full set of parameters.
 [DOI: 10.1149/1945-7111/ac26b1]

Manuscript submitted May 1, 2021; revised manuscript received August 25, 2021. Published September 23, 2021.

Supplementary material for this article is available online

Lithium-ion batteries have become ubiquitous in modern technology including in personal consumer devices and automobiles. Batteries are commonly modeled using porous electrode theory (PET),[1] which includes electrochemical kinetics at the solid-electrolyte interfaces in the porous electrodes, transport through the electrolyte and in the solid particles, and thermodynamics modeled by an algebraic function for the open-circuit potential. The PET model is commonly referred to as a "pseudo-two-dimensional" (P2D) model, in which one dimension is the position between the two metal contact points on the opposite sides of the electrode-separator-electrode sandwich and the second dimension is the distance from the center of a solid particle. The common practice is to fit a half dozen effective transport and kinetic coefficients in the PET model to battery cycling data,[1] and then to use the model to explore changes in the battery design or the operating conditions.

An important consideration when fitting model parameters to experimental data is whether the data contain sufficient information content to uniquely specify the model parameters. Answering this question is referred to as an *identifiability analysis*. Past works have employed structural and linearized identifiability analyses to show that multiple combinations of effective transport and kinetic coefficients can produce nearly identical voltage discharge curves. This article takes an alternative approach of carrying out a fully nonlinear quantitative identifiability analysis for the PET model. This approach provides very precise information on the uncertainty of the combinations of estimated model parameter, and to make precise statements as to which of the original model parameters are unlikely to be practically identifiable for commercial lithium-ion batteries.

Numerous publications have fit various lithium-ion battery parameters to cycling data using different models and methods. For example, a local linearized sensitivity analysis was applied to separate groups of thermodynamic and kinetic PET model parameters regressed on low-current discharge curves and current pulses respectively.[2] Jokar et al.[3] implemented a local linearized sensitivity analysis, which was coupled with a genetic algorithm applied to a simplified P2D model to establish the time periods where parameters greatly affect a voltage discharge curve under high and low C-rates. Another study[4] applied linearized local sensitivities and a Monte Carlo-based covariance analysis to study identifiability from discharge curves and the electrolyte concentration in the center of the separator. A fit of a hundred PET model parameters to experimental battery cycling data using a genetic algorithm[5] found that only a small subset of the parameters were identifiable. The identifiability of parameters in the single-particle (SP) model with electrolyte dynamics under constant state of charge (SOC), represented in terms of probability density functions of model parameters, has been quantified by Markov chain Monte Carlo (MCMC).[6] Unidentifiability in the solid-state diffusion parameters was alleviated by applying a sinusoidal pulse to achieve a range of SOC. At low C-rates, the SP model has comparable error to the P2D model.[7] The MCMC method has also been applied to quantify uncertainties in five effective transport and kinetic coefficients in the PET model.[8] Reductions in the effective transport and kinetic coefficients over the cycle life of a Li-ion battery were plotted and shown to follow a power law. The approach predicted voltage discharge profiles at future cycles from experimental data collected for the first 200 cycles.

This article considers the question of whether the effective model parameters in the PET model fit to voltage discharge curves actually converge to their true values. Resolving this question is important when attempting to draw a connection between changes in the effective model parameters with cycle number and the true physicochemical changes occurring in the battery. The nonlinearity identifiability analysis in this article quantifies precisely what can be learned from such fitting, what cannot be learned, about battery kinetics and transport from fitting the model parameters to battery cycling data.

Background

Porous electrode theory (PET).—Porous Electrode Theory (PET) was developed by Newman and collaborators at the University of California, Berkeley.[1,9–11] Each porous electrode has an electrically conductive solid phase in close contact with a liquid electrolyte. Lithium ions are dynamically transported between active particles in the electrolyte described by Fickian diffusion and Ohmic conduction. The two phases are coupled by interfacial electrochemical kinetics, typically modeled in the literature by Butler-Volmer kinetics but adaptable to Marcus theory. Solid-phase transport is assumed to be Fickian. The PET model is commonly referred to as being "pseudo-two-dimensional (P2D)," in which one dimension is

[z]E-mail: braatz@mit.edu

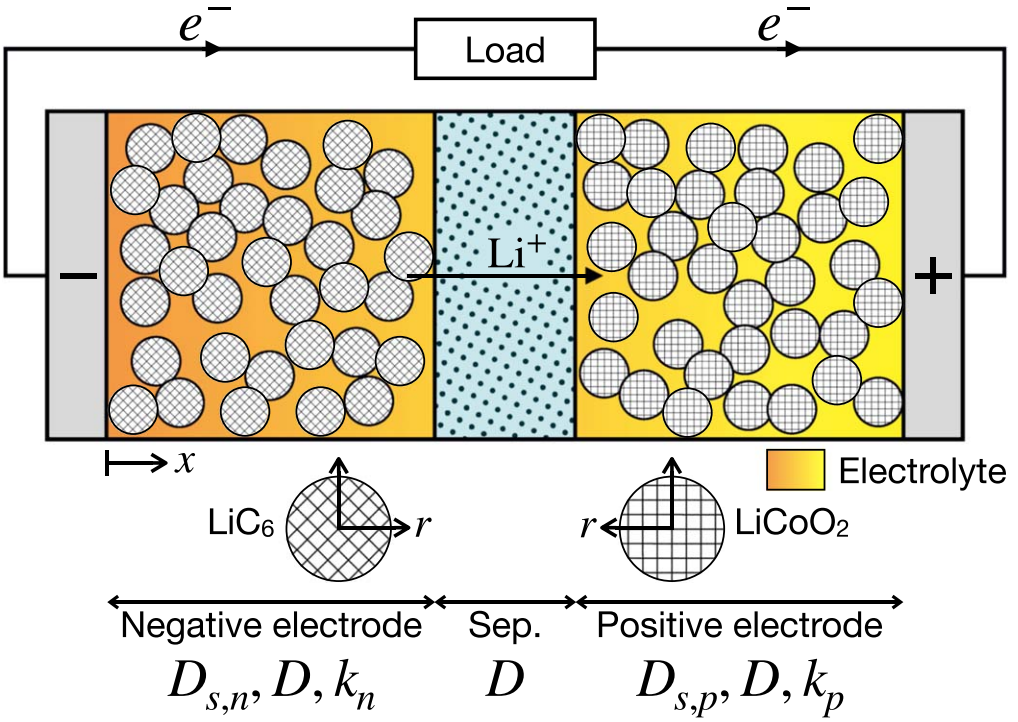

Figure 1. Schematic of the PET model for an $LiC_6/LiCoO_2$ cell during discharge. The parameters of interest in θ are listed under the sections whose physics they principally affect. The vector of model parameters θ consists of the effective solid-phase diffusion coefficients ($D_{s,n}$ and $D_{s,p}$, m^2/s), the effective electrolyte diffusion coefficient (D, m^2/s), and the effective reaction rate constants (k_n and k_p, $m^{5/2}/(mol^{1/2}s)$.)

the position between the two metal contact points on the opposite sides of the electrode-separator-electrode sandwich and the second dimension is the distance from the center of a solid particle (Fig. 1).

Many software implementations of PET have been developed.[12–15] This article uses LIONSIMBA,[16] which is a MATLAB implementation of the PET model based on the finite volume method. The finite volume method has (1) exact handling of flux boundary conditions and total conservation of all conserved variables (e.g., Li atoms) throughout the control volume, and (2) relatively simple implementation compared to the finite element method, making the software easier for users to modify. Numerical results of the LIONSIMBA implementation agree with DUALFOIL from the Newman group and COMSOL MultiPhysics.

Maximum likelihood estimation.—Uncertainties in parameter estimates can be quantified by probability density functions (PDFs) using Bayesian inference, which relates a *posterior distribution* $P(\theta|Y)$ to the experimental data Y and the prior distribution $P(\theta)$ of the model parameters θ via

$$P(\theta|Y) = \frac{P(Y|\theta)P(\theta)}{P(Y)} \quad [1]$$

where Y is the vector of measurements y_j, $P(Y|\theta)$ is defined below, and $P(Y)$ is a constant that normalizes the posterior distribution to have its integral equal to one. When no prior knowledge is available, then the prior distribution $P(\theta)$ is set to a constant.

For zero-mean normally distributed noise, the probability of observing the vector of measurements Y, given a vector of model parameters θ, is

$$P(Y|\theta) = \prod_{j=1}^{N_d} \frac{1}{\sigma_\epsilon \sqrt{2\pi}} \exp\left(-\frac{1}{2}\left(\frac{y_j - \hat{y}_j(\theta)}{\sigma_\epsilon}\right)^2\right), \quad [2]$$

where N_d is the number of experimental observations and σ_ϵ is the standard deviation of the measurement error for the output y_j. Under the above assumptions, the calculations for determining the maximum-likelihood (ML) estimates can be simplified by using a logarithmic transformation[17]

$$\begin{aligned}
\theta^*_{ML} &= \arg\min_\theta(-2\ln(P(\theta|Y)) \\
\theta^*_{ML} &= \arg\min_\theta\Big(N_d \ln(2\pi\sigma_\epsilon^2) \\
&\quad + \sum_{j=1}^{N_d}\left(\frac{y_j - \hat{y}_j(\theta)}{\sigma_\epsilon}\right)^2 - 2\ln P(\theta) + 2\ln P(Y)\Big) \\
\theta^*_{ML} &= \arg\min_\theta \sum_{j=1}^{N_d}\left(\frac{y_j - \hat{y}_j(\theta)}{\sigma_\epsilon}\right)^2. \quad [3]
\end{aligned}$$

This argument is commonly employed in parameter estimation and referred to as minimizing the sum of squared residuals.[17]

Maximum a posteriori estimation.—Maximum *a posteriori* (MAP) estimation combines experimental data with prior information about the parameter values to obtain a better joint estimate than ML estimation alone.[17,18] The objective $-2\ln P(\theta|Y)$ is minimized to obtain the best estimate for the parameters θ, as in ML estimation, but prior information on θ is used (such as past experimental values in the literature) and $P(\theta)$ is no longer a constant. For normally distributed parameters and zero-mean normally distributed noise:

$$\begin{aligned}
\theta^*_{MAP} &= \arg\min_\theta(-2\ln P(\theta|Y)) \\
\theta^*_{MAP} &= \arg\min_\theta\Bigg(N_d \ln(2\pi\sigma_\epsilon^2) + \sum_{j=1}^{N_d}\left(\frac{y_j - \hat{y}_j(\theta)}{\sigma_\epsilon}\right)^2 \\
&\quad + \sum_{i=1}^{N_p}\left(\ln(2\pi\sigma_{\mu,i}^2) + \left(\frac{\theta_i - \mu_i}{\sigma_{\mu,i}}\right)^2\right) + 2\ln P(Y)\Bigg) \\
\theta^*_{MAP} &= \arg\min_\theta \sum_{j=1}^{N_d}\left(\frac{y_j - \hat{y}_j(\theta)}{\sigma_\epsilon}\right)^2 + \sum_{i=1}^{N_p}\left(\frac{\theta_i - \mu_i}{\sigma_{\mu,i}}\right)^2 \quad [4]
\end{aligned}$$

where i is the parameter index, N_P is the number of parameters, and μ, $\sigma_\mu \in \mathbb{R}^{N_p}$ are the vectors of prior parameter values and standard deviations respectively. The latter term in Eq. 4 can be interpreted as being a regularization term. When the prior parameter estimates are accurate (small $\sigma_{\mu,i}$) then the MAP estimates will be close to the priors. On the other hand, if the prior knowledge is highly uncertain (large $\sigma_{\mu,i}$) then the MAP estimates can be quite different from the prior parameter value μ_i.

In the absence of *prior* information (i.e., an infinitely large standard deviation of parameter values), MAP estimation converges to ML estimation:

$$\lim_{\sigma_{\mu,i}\to\infty} \theta^*_{\text{MAP}} = \theta^*_{\text{ML}}. \quad [5]$$

Parameter identifiability analysis.—Before carrying out a model identification for a complex system, a parameter identifiability analysis should be performed to determine whether the model structure, noise level, and operating regime allow the model parameters to be estimatable from the experimental data.[19] Parameters are said to be *identifiable* if estimatable from the observed data. Unidentifiability of a model can be broadly classified in two ways: *structural unidentifiability*, where parameter groupings in the set of modeling equations cannot be solved uniquely and *practical identifiability*, where regressing parameters against empirical data leads to non-unique results.[17] Practical unidentifiability occurs when the observed data are not sufficiently informative to be able to estimate unique values for the model parameters. In complex physicochemical systems with limited experimental data, it is common for some model parameters to be practically unidentifiable.

A parameter is practically identifiable if its confidence interval is finitely bounded. If its confidence interval is infinite when increasing and/or decreasing, then the parameter is practically unidentifiable. Unidentifiable models may contain several different *identifiable combinations* which include parameters that are individually unidentifiable.[20] Examples of different practical identifiabilities are shown in the Example Confidence Regions section. The results of an identifiability analysis depends on the choice of the type of experimental data and the quantity and quality of the data in addition to the model.

Estimating sets of model parameters in highly nonlinear battery models with identifiability issues can be computationally expensive and may produce misleading aphysical results. Past papers in the electrochemical literature have characterized parameter identifiability via sensitivity analyses with some cutoff sensitivity value to determine practically unidentifiable parameters (e.g.,[21]). However, such linearized methods can produce inaccurate results. Evaluating sensitivities for several different θ^* may lead to greatly different results despite all providing great fits to the nominal solution, for example. A more detailed assessment of the nonlinear parameter confidence region should be made to fully understand the effect of parameters on the model outputs.

Confidence regions.—This section summarizes methods for computing confidence regions from models and experimental data.

Linearized confidence regions.—For linear and nearly linear systems of equations with normally distributed noise, a confidence region for quantifying uncertainty in estimated model parameters can be described by a hyperellipsoid in a subset or full set of parameters θ. The first step in construction of a confidence region is to compute the best estimate of parameters θ^*, usually by minimizing the sum of squared residuals and maximizing the likelihood function (that is, determining the vector of parameters that have the highest likelihood based on the data).[17] The first-order Taylor expansion around θ^* is

$$\hat{y}_j(\theta) \approx \hat{y}_j(\theta^*) + F_j(\theta^*)(\theta - \theta^*) \quad [6]$$

where the sensitivity matrix F_j given by

$$F_j = \left.\frac{\partial \hat{y}_j}{\partial \theta}\right|_{\theta^*} \quad [7]$$

can be computed with finite differences, a forward sensitivity analysis, or an adjoint sensitivity analysis for all observed outputs and parameters. Sensitivities are often used in optimization algorithms for the numerical solution of θ, including gradient descent, conjugate gradient, and sequential quadratic programming.[22] Sensitivity analyses are also used as a means to reduce the parameter space by establishing statistical significance with a sensitivity cutoff.[17,21,23,24]

The confidence region can be approximated by the hyperellipsoid[25] (e.g., Fig. 2a),

$$\{\theta\colon (\theta - \theta^*)^\top V_\theta^{-1}(\theta - \theta^*) \leqslant \chi^2_{N_p}(1-\alpha)\}, \quad [8]$$

where χ^2 is the chi-squared distribution, α is the level of significance, $^\top$ refers to the matrix transpose, and the parameter covariance matrix is given by

$$V_\theta^{-1} = \sum_{j=1}^{N_d} F_j^\top V_\epsilon^{-1} F_j. \quad [9]$$

A common assumption is that measurement errors are normally distributed and independent of each other,[17] in which case the measurement covariance matrix is diagonal with $V_{\epsilon,ii} = \sigma_i^2$.

Finite sample confidence regions.—While the above formulation is appropriate for linear or nearly linear systems, local sensitivity analyses can produce misleading results for nonlinear systems of equations. For example, consider a hyperellipsoid linearized around θ^*. For the common assumptions that measurement errors are normally distributed and independent, the linearized confidence

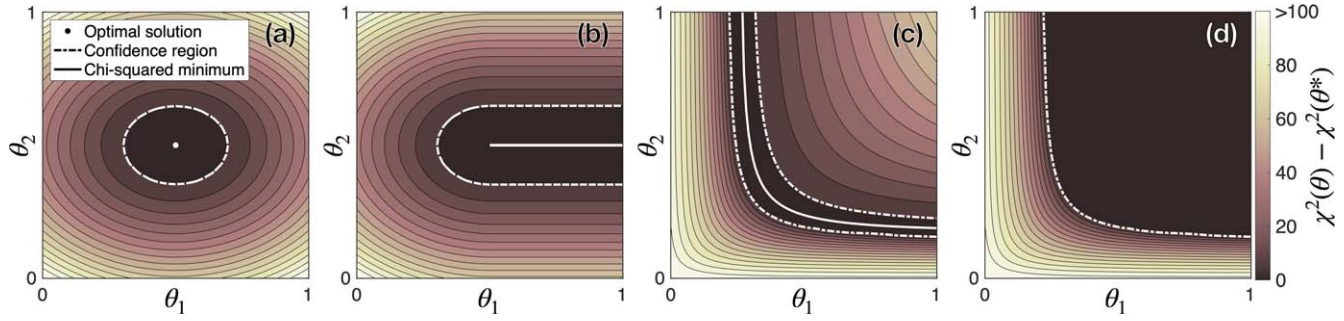

Figure 2. Example chi-squared distributions for (a) a pair of identifiable parameters, (b) one unidentifiable and one identifiable parameter, (c) a pair of (globally) unidentifiable parameters that are locally identifiable, and (d) a pair of simultaneously unidentifiable parameters. The chi-squared minimum is a manifold of optimal solutions where the error is minimized.

region is guaranteed to be convex and centered around θ^* (since V_ϵ is a positive definite matrix), leading to a global minimum at θ^*. Such a representation is not applicable to systems that are practically unidentifiable, since these systems have infinitely many feasible solutions for θ^*.

Electrochemical systems can have highly nonlinear relationships between the model parameters and the model predictions, which can result in linearized statistical analysis producing inaccurate results.[26] The uncertainty in the estimated parameters for nonlinear models will not necessarily be accurately portrayed by a hyperellipsoid. A general confidence region can be computed using a more computationally expensive approach. The chi-squared distribution is related to the best estimate of the parameters by the log-likelihood function.[27] For normally distributed zero-mean noise, the chi-squared distribution is

$$\chi^2(\theta) = \sum_{j=1}^{N_d} \left(\frac{y_j - \hat{y}_j(\theta)}{\sigma_\epsilon} \right)^2, \qquad [10]$$

which is equivalent to ML estimation in Eq. 3. A nonlinear confidence region is described by all θ that satisfy the inequality[17,28]

$$\{\theta: \chi^2(\theta) - \chi^2(\theta^*) \leqslant \chi^2_{N_p}(1-\alpha)\}. \qquad [11]$$

A simple algorithm for the nonlinear case is to evaluate the model for all points in a grid of values of θ^* in parameter space. To obtain a quantitative understanding of the effects of nonlinearity on the shape of the conference region, this equation can be computed for many values of α, e.g., 0.01, 0.05, 0.10 would correspond to the 99%, 95%, and 90% confidence regions respectively. This method of quantifying the uncertainty in parameter estimates is more computationally expensive than using V_θ^{-1}, which only requires a small number of function evaluations to compute the sensitivity matrix, but the extra information is valuable when the system is highly nonlinear.

Markov chain monte carlo (MCMC).—Monte Carlo methods are well-known techniques for randomly sampling from probability density functions (PDFs) to compute an integral or estimate distributions where deterministic approaches are not possible.[29–31] Markov chain Monte Carlo (MCMC) is a method for uncertainty quantification for nonlinear models.

The Metropolis-Hastings algorithm allows for efficient sampling of the PDFs.[32] Parameters are initialized at θ_0 and random perturbations to the parameters are applied.[33] An objective function $f(\theta)$, such as the sum of squared residuals or $\chi^2(\theta)$, is evaluated at each iteration t. The step is either accepted or rejected, typically based on an acceptance ratio a for a proposed step θ'.

Example confidence regions and interpreting identifiability.—Four example confidence regions which may appear in nonlinear models (such as porous electrode battery models[1,16,34]) are shown in Fig. 2. In these examples, $\theta \in \mathbb{R}^2$—other visualization methods such as isosurfaces and subplots may be used to view higher dimensional parameter spaces.

Figure 2a shows the confidence region for two identifiable parameters and an optimal solution θ^*. These parameters are identifiable since θ^* is finitely bounded. A linearized confidence region is appropriate for this set of parameters.

In Fig. 2b, θ_1 is unidentifiable and θ_2 is identifiable. The chi-squared minimum can be thought of as "stretching" the optimal solution point into a line. Along this line, infinitely many θ^* values exist for increasing θ_1. Following the chi-squared minimum line, a confidence interval for θ_1 would extend toward $+\infty$. The parameter θ_2, on the other hand, is identifiable since its confidence region is finitely bounded. Optimizing the objective function for θ with several different initial guesses may lead to puzzling results since θ_1^* is not unique. If the confidence region was linearized at any point along the chi-squared minimum, the result would inaccurately look like an elongated version of Fig. 2a.

Figure 2c shows two parameters that are globally unidentifiable and the chi-squared minimum curve that lies within all of the confidence regions. A banana-shaped confidence region is often seen for highly nonlinear models[17] in which an infinite number of parameter values gives either the same or nearly the same quality of fit. The parameter would appear to be locally identifiable, in that a numerical optimization at any initial guess would converge to a point on the minimum curve that would locally appear to be minimum over θ_1 for fixed θ_2 and locally appear to be minimum over θ_2 for fixed θ_1. Inspection of the conference regions as a function of both parameters, as seen in Fig. 2c, shows that the two parameters are not globally identifiable. The two extremes of the minimum curve, where $\theta_1 \to \infty$ and $\theta_2 \to \infty$ respectively, show very different sensitivities on θ_1 and θ_2. Sensitivities of the parameter estimation objective on the parameters can be very large or nearly zero depending on the value of the other parameter. This observation has strong implications in parameter estimation, and implies that only relying on local sensitivities can lead to misleading results.

The two parameters in Fig. 2d are both unidentifiable. The darkly shaded region above the confidence interval is the chi-squared minimum plane where infinitely many solutions in $\mathbb{R}^2$ exist.

Identifiability Methodology

The nonlinear identifiability analysis in this article consists of three steps: (1) apply Bayesian estimation for θ using MCMC, (2) find practically identifiable and unidentifiable parameters from the probability densities, and (3) further classify the identifiable combinations with a gridded mesh of chi-squared values. Once the parameter space is thoroughly mapped, the set of identifiable parameter groups are established which contain all identifiable and some locally identifiable parameters.

Optionally, the parameter space may be reduced by fixing unidentifiable parameters to an estimate or physically meaningful upper/lower bound. In a similar manner, equations deemed unimportant due to the unidentifiable parameters may be removed from the model for computational efficiency. For example, a very thin porous electrode that is not diffusion limited could have the effects of diffusion in the porous electrode removed from the model. A less restrictive option is to add a prior value from the literature.

Practical identifiability is confirmed from the results of Bayesian estimation. If a sufficiently large number of Markov chains indicate that the parameter is finitely bounded, then the parameter is practically identifiable. If the chains includes parameter values that are arbitrarily small or large, then the parameter is practically unidentifiable; whether the parameter is in any identifiable combinations necessitates more investigation. The set of all identifiable combinations contain every practically identifiable parameter.

Locally identifiable parameters which form *identifiable combinations* are first assessed from their probability densities. If the probability density for a parameter has a (1) a large peak and (2) a lower magnitude plateau for larger or smaller values of the parameter, then the parameter is likely in the set of identifiable combinations while still being practically unidentifiable. The large peak comes from identifiable combinations which involve the parameter. The plateau is due to the identifiable combinations which do not involve the parameter, i.e., where the parameter is unidentifiable. Parameters with a uniform probability density are not in any sets of identifiable combinations.

While Bayesian estimation gives a rough idea about the identifiability trends, mapping out the nonlinear confidence region is required to definitively classify identifiable combinations (e.g., Fig. 2). Plotting the gridded nonlinear confidence region will exhibit the regions where practically unidentifiable parameters can infinitely increase and/or decrease. Moreover, it is helpful for classifying

identifiable combinations at extreme points in parameter space, such as in Fig. 2c.

Model Specifications

The transport and kinetic parameters considered in this article are $\theta = [D_{s,p}, D_{s,n}, D, k_p, k_n]^T$, where $D_{s,p}$ and $D_{s,n}$ are the effective solid-phase diffusion coefficients of Li in the cathode and anode respectively, D is the effective diffusion coefficient in the electrolyte, and k_p and k_n are the effective electrochemical reaction rate constants for the cathode and anode respectively. The region of the battery that each parameter primarily acts on is shown under the section headers in Fig. 1. These parameters are *effective*, that is, they lump the effects of multiple true material properties together.[9] The effective electrolytic diffusivity lumps together the species' molecular diffusivity and the media's porosity, tortuosity, and constrictivity. The effective kinetics lump together the true kinetic parameters and available surface area.

To ensure that identifiability results are relevant to real lithium-ion batteries, the physical specifications of the LCO/LiC_6 battery are provided by Ramadesigan et al.[8] To gain insights into potential biases occurring during parameter estimation, the identifiability analysis is applied to a synthetic voltage discharge curve at a C-rate of C/10 generated in LIONSIMBA (see Fig. 3) with $\epsilon \sim \mathcal{N}(0, \sigma_\epsilon^2)$, where $\sigma_\epsilon = 10$ mV is the standard deviation of the voltage measurement noise. The parameter estimation optimizations were performed on a logarithmic basis of θ, which is a standard approach used to improve numerical convergence for parameters that can change by many orders of magnitude.

The particular MCMC variant used in this study is Delayed Rejection Adaptive Metropolis (DRAM) implemented by Haario et al.[32] which combines Adaptive Metropolis (AM) samplers with Delayed Rejection (DR) for numerical efficiency. Identifiability is indirectly assessed by running multiple parallelized MCMC iterations to sample from the probability density in θ. The MCMC objective function uses ML estimation in Eq. 3.

Results and Discussion

Bayesian estimation.—The histograms of the probability densities of the model parameters θ generated using MCMC (Fig. 4) indicate that the only finitely bounded parameter in this experimental setup is the solid-phase effective diffusion coefficient $D_{s,n}$, meaning that $D_{s,n}$ is practically identifiable and operating in a diffusion-limited regime at this discharge rate. The other four parameters $D_{s,p}$, D, k_p, and k_n all approach the imposed upper limit of 10^{-7} and are practically unidentifiable from the voltage discharge curve. Some kinetic and diffusive parameters becoming unidentifiable for large values is consistent with the associated phenomena not being rate-limiting. At higher C-rates, diffusion will have a different impact on the voltage discharge curve leading to different identifiability trends. The same methodology outlined in this article also applies to these conditions. The probability densities for four out of five parameters have peak values that are significantly smaller than their true values (shown in (Figs. 4a, 4c–4e) and quantified in Table I), meaning that a parameter estimation procedure fit to experimental data would likely underestimate the true values of those model parameters. In other words, the values for the parameter estimates corresponding to the peaks of the probability densities for four of the parameters fit to a voltage discharge curve can be highly biased—much smaller than the true values. This phenomena can be considered as an additional type of limitation to the identifiability of those model parameters. The reduced identifiability for small values of the four parameters can be explained physically by noticing that the voltage-current relationship is governed by the overall flow of lithium ions across the battery, which is akin to resistances in series. Small values of each of the four parameters can be consistent with the voltage discharge curve, as long as some other parameter values are large enough that the overall lithium ion flow is consistent with the data.

Of the four unidentifiable parameters, the distribution of $D_{s,p}$ is the most uniform: the probability density near 10^{-14} is the same order of magnitude as the probability density near the upper bound. Since it is nearly as probable to find $D_{s,p}$ in expansive areas in parameter space, the parameter is strongly unidentifiable. The peaks for the other unidentifiable parameters D, k_p, and k_n, are similar in scale and appearance to each other. In contrast to $D_{s,p}$, the probability density peaks are an order of magnitude larger than the plateau at the upper bound. From an identifiability perspective, these parameters are likely involved in some identifiable combinations and are locally identifiable near their Bayesian estimation peak. While locally identifiable, the non-zero plateau signifies that these parameters are also practically unidentifiable.

Histograms only provide broad information into identifiability trends. While $D_{s,p}$, D, k_p, and k_n are all unidentifiable to varying degrees, the particular combinations of parameters that are identifiable cannot be determined directly from probability densities. A detailed nonlinear identifiability analysis is required to answer this question, which is provided in the next section.

Nonlinear identifiability analysis.—Bayesian estimation shows that (1) $D_{s,n}$ is identifiable and (2) D, k_p, and k_n are potentially locally identifiable for a C/10 discharge. To find the identifiable

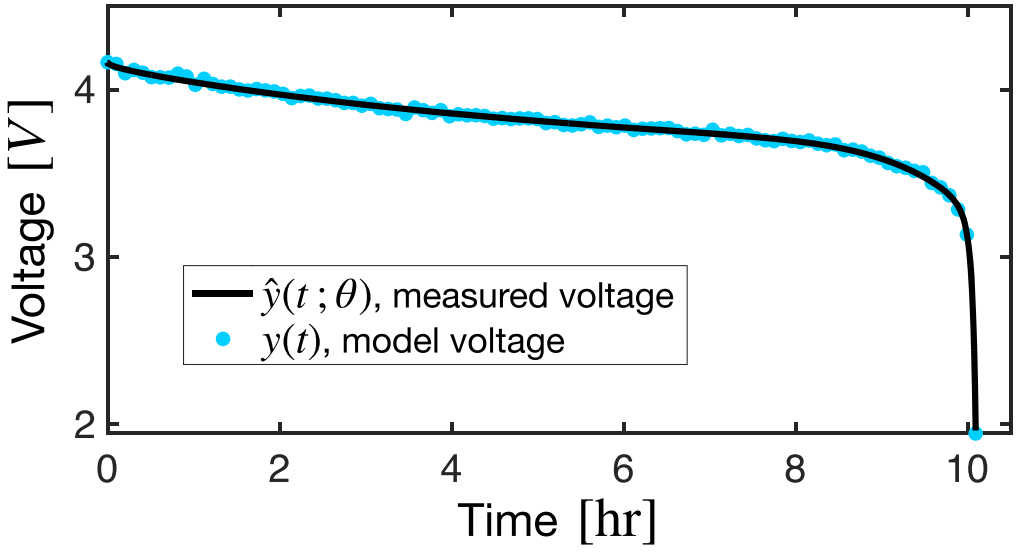

Figure 3. LCO/LiC_6 discharge curve at a C-rate of C/10 with synthetic data and model fit.

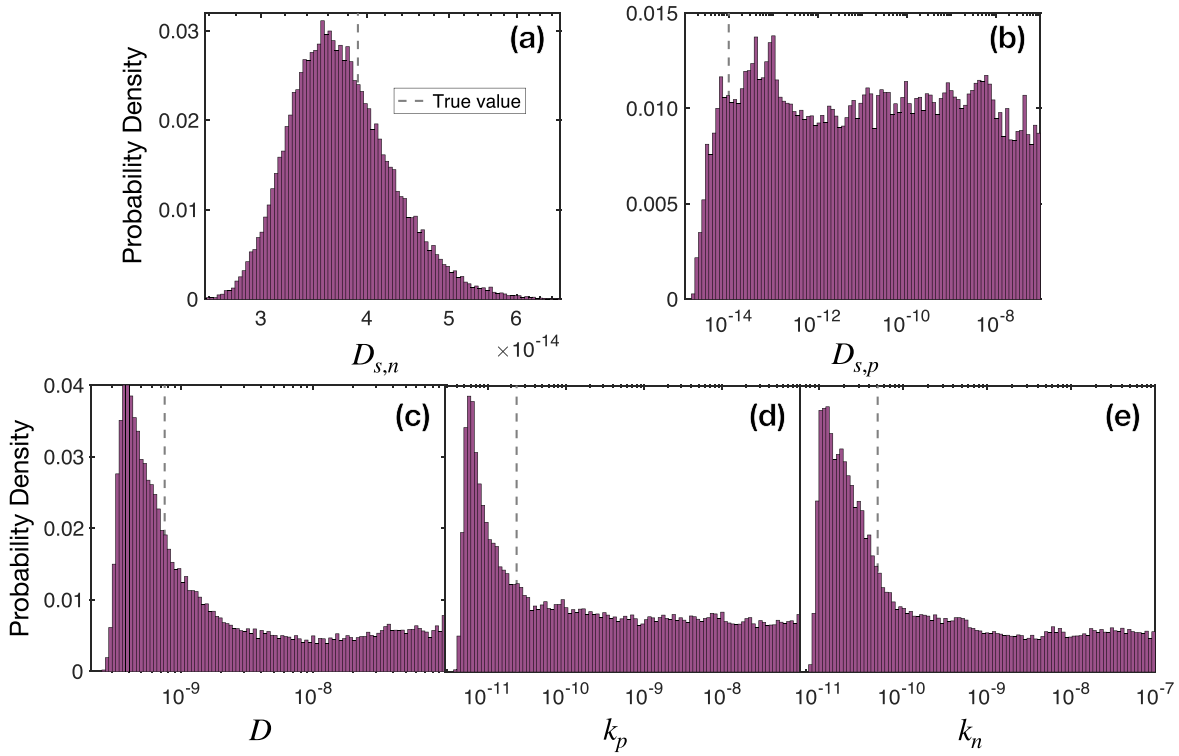

Figure 4. Probability densities of the θ_j determined by MCMC: (a) $D_{s,n}$ is the only parameter that can be finitely bounded, and is the only practically identifiable parameter. (b) $D_{s,p}$ has a nearly uniform probability density and is practically unidentifiable. (c)–(e) D, k_p, and k_n have a large peak, likely meaning they are contained in some identifiable combinations, and plateau toward their upper bound, meaning they are practically unidentifiable. The parameter vector θ was bounded between 10^{-20} and 10^{-7} to prevent unidentifiable parameters from becoming too large.

Table I. Bayesian estimation results from MCMC.

	Bayesian estimation peak	Confidence interval (95%)
$D_{s,p}$	1.01e–13	[1.49e–15, $+\infty$[a)]]
$D_{s,n}$	3.54e–14	[2.58e–14, 6.76e–14]
D	3.71e–10	[2.57e–10, $+\infty$[a)]]
k_p	5.76e–12	[3.73e–12, $+\infty$[a)]]
k_n	1.28e–11	[7.83e–12, $+\infty$[a)]]

a) An upper limit of 10^{-7} was set for all parameters in MCMC. If the upper bound was reached, it was subsequently verified when approaching $+\infty$.

combinations of parameters, $D_{s,n}$ is set to its Bayesian estimation peak and each of the suspected locally identifiable parameters are individually set to their peak. All other parameters that are not fixed can be set to an arbitrarily large number (10^{-3}) to represent the case where they are practically unidentifiable.

Pairwise combinations of parameters that are identifiable should be determined from plots of the confidence regions. Three identifiable combinations are shown in Fig. 5: (a) $D_{s,n}$ & D, (b) $D_{s,n}$ & k_p, and (c) $D_{s,n}$ & k_n. The finitely bounded confidence regions means these identifiable pairwise combinations satisfy the nominal solution. The optimal solution of each identifiable combination (Table II) occurs near the Bayesian estimation peak, indicating that these pairs of parameters are locally identifiable. For each choice of two parameters, the three other parameters in θ have a negligible effect on the objective function, and therefore will have sensitivities approaching zero. Optimal parameter estimates may belong to any of these identifiable pairwise combinations, but the sensitivities evaluated at θ^* will be vastly different. These results highlights the point that local derivatives sensitivity and confidence region calculations can be misleading when applied to lithium-ion batteries fit to voltage discharge curves. Many papers have applied local sensitivity analyses (e.g.,[2–4]) to estimate a set of locally identifiable parameters, but such analyses should not be used to make conclusions on the parameter space at large.

A past study[8] found that, for the same set of five parameters considered in this article, capacity fade could be predicted for future cycles while only regressing $D_{s,n}$ and k_n. Large uncertainties observed for $D_{s,p}$, D, and k_p were addressed by fixing their values to be constants, and reductions in the estimated $D_{s,n}$ and k_n with cycle number were observed to follow a power law. Although the approach[8] was successful in accurately predicting future voltage discharge curves, the above nonlinear identifiability results indicate that the observed reductions in $D_{s,n}$ and k_n with cycle number may not necessarily be attributable to degradation in the negative electrode.

Useful insights can be obtained by plotting the isosurfaces for the three locally identifiable parameters D, k_p, and k_n (Fig. 6). The isosurfaces enable a higher dimensional understanding of the identifiability relationship between the three parameters. The isosurface can be interpreted as stacking 2D confidence regions to show how the confidence region varies with an additional parameter. As in Fig. 5, the unidentifiable parameter $D_{s,p}$ is set to a large value, and the identifiable parameter $D_{s,n}$ is set to its Bayesian estimation peak. The isosurface looks similar for all values of $D_{s,p}$ above the lower bound (not shown for brevity), below which the isosurface does not exist.

The isosurface has noted symmetry when approaching the lower bounds of D, k_p, and k_n which mirror the similarities seen in their probability densities (Figs. 4c–4e). These results are expected: if the confidence regions where the parameters are locally identifiable are similar then it follows that their probability densities should look similar. Moreover, the three-fold symmetry

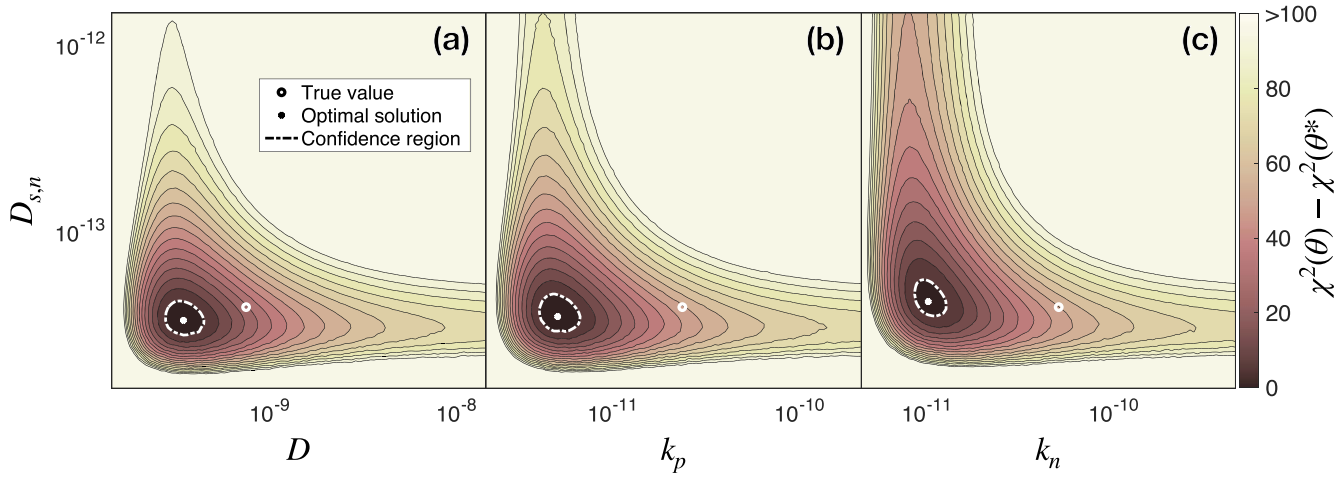

Figure 5. Local confidence regions of two parameters in θ, where the three parameters excluded from each plot are set to 10^{-3}. Three identifiable combinations exist, each containing two parameters: (a) $D_{s,n}$ & D, (b) $D_{s,n}$ & k_p, and (c) $D_{s,n}$ & k_n. The confidence interval is $\chi^2_2(0.95) = 5.99$.

Table II. Local statistics for the three identifiable combinations from the results of Fig. 5 and an unidentifiable combination ($D_{s,n}$ and $D_{s,p}$). Each combination contains two parameters in θ; the other three parameters are made arbitrary large since they are practically unidentifiable.

θ_1	θ_2	Optimal solution		Local confidence interval (95%)	
		θ_1	θ_2	θ_1	θ_2
$D_{s,n}$	D	3.32e–14	3.47e–10	[2.76e–14, 4.21e–14]	[2.78e–10, 4.46e–10]
$D_{s,n}$	k_p	3.47e–14	5.03e–12	[2.89e–14, 4.59e–14]	[4.01e–12, 6.63e–12]
$D_{s,n}$	k_n	4.18e–14	1.01e–11	[3.49e–14, 5.49e–14]	[8.54e–12, 1.26e–11]
$D_{s,n}$	$D_{s,p}$	3.88e–14	1.98e–15	—	—

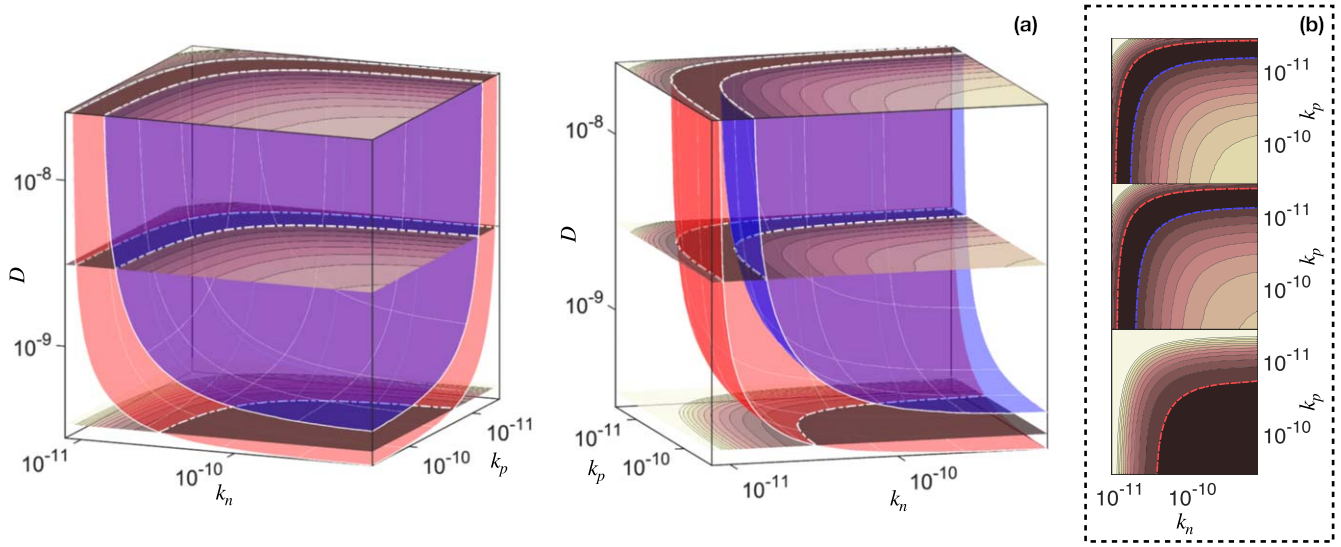

Figure 6. Isosurfaces of the 3D confidence regions showing two perspectives (a) and 2D slices for three values of constant D (b). The isosurface is equivalent to stack of 2D confidence regions where the curved lines correspond to the 95% confidence interval. The shape qualitatively resembles the sum of resistances in series (Eq. 12) between locally identifiable parameters. The red and blue sections are the lower and upper bound of the confidence regions respectively. An interactive version of the figure is available at https://marcberliner.github.io/PET-isosurface/. The k_p axis is reversed for visual clarity.

of the isosurface (as shown in Fig. 1 (available at stacks.iop.org/JES/168/090546/mmedia)) speaks to the similar effects that varying these three parameters has on the voltage discharge curve: diffusion and rate constants affect how quickly Li moves across the length of the battery in particular sections. Like resistances in series (resistance to Li-ion flow is inversely proportional to D and k), these parameters must be simultaneously tuned so that Li moves at the appropriate rate through the battery. Modeling a functional relationship for the locally identifiable parameters as resistances in series gives the relationship

Table III. Fitting constants in Eq. 12.

β_D	β_{k_p}	β_{k_n}
4.08e–10	4.06e–12	8.55e–12

Table IV. Values of prior means and standard deviations on a logarithmic basis. Reported transport and kinetic parameters are concentration dependent—a constant value was obtained from a weighted-average of the data.

	$\log_{10}\mu_i$	$\log_{10}\sigma_{\mu,i}$	References
$D_{s,p}$	−15.26	0.2513	36
$D_{s,n}$	−11.63	0.2841	37
D	−9.490	0.1496	38
k_p	−12.49	0.3007	39
k_n	−9.736	0.3283	40

$$1 = \frac{\beta_D}{D} + \frac{\beta_{k_p}}{k_p} + \frac{\beta_{k_n}}{k_n}, \quad [12]$$

where β_D, β_{k_p}, β_{k_n} are positive fitting constants. The chi-squared minimum manifold can be estimated by regressing Eq. 12 against the isosurface data. The numerical values of the fitted constants in Table III are close to the lower bounds for D, k_p, k_n in Tables I and II, which is consistent when considering the contours of the isosurface and rate-limiting behavior of the parameters. The values of D, k_p, k_n all asymptotically approach some value when $\chi^2(\theta) - \chi^2(\theta^*)$ is fixed. When two of the three practically unidentifiable parameters are driven to $+\infty$, the other parameter asymptotically approaches its corresponding fitting constant, for example,

$$\lim_{k_p,k_n\to\infty} D = \beta_D \quad [13]$$

and likewise for k_p and k_n.

While D, k_p, and k_n are all locally identifiable, their large uncertainties when fit to voltage discharge curves imply that physical meaning cannot be inferable from the practically unidentifiable parameters. Large biases can occur by propagating error from the other unidentifiable parameters onto the locally identifiable parameter, which can result in the values of D, k_p, k_n estimated from voltage discharge curves to be *lower* than their true values (Fig. 6). Each individual parameter is only locally identifiable when the other two parameters are made large (e.g., see the top portions of the plots in Fig. 6) and subsequently has little to no effect on the total resistance in series, and each locally identifiable parameter asymptotically approaches its *lower bound* to match the appropriate resistance to lithium-ion flow. The true solution is near the point of highest curvature in the isosurface in Fig. 6, which is incorrectly estimated in both MCMC and the nonlinear contour plots. Since the practically unidentifiable parameters are dependent on each other, only the total resistance to lithium-ion flow is unique and identifiable.

Removing practical unidentifiabilities.—Some approaches to deal with unidentifiable parameters are (1) setting such parameters to constant values, (2) adding a prior term to the objective function, (3) model reduction (or removing the equations involving the parameters), and/or (4) collecting more informative datasets. Any approach for reducing θ to an identifiable combination can be used to ensure that the parameter estimation has a unique global minimum.

Table V. Global minima for the identifiable combinations. The baseline for the normalized objective function is the five-parameter Bayesian estimation result.

Identifiable combination	Normalized objective function
$D_{s,n}$ & D	24.9
$D_{s,n}$ & k_p	1.54
$D_{s,n}$ & k_n	29.4

1. Fixing parameters to constants. A simple method of removing unidentifiabilities is to fix the parameters to constants. The constants can be estimated from computational chemistry calculations or empirical studies in the literature for the same or closely related systems. Parameters which are not in any identifiable combinations simply can be fixed to any value contained within its confidence interval. The number of degrees of freedom in the parameter estimation optimization is reduced, which reduces the associated computational cost. With locally identifiable parameters, it is necessary to ensure that fixing the parameters to constants do not make the parameter estimation problem numerically poorly conditioned. In particular, all of the fixed parameters must be contained within the nonlinear confidence interval (such as the isosurface in Fig. 6a).

A drawback of fixing parameters to constants is that the estimates for parameters may vary from different sources. For example, estimates for $D_{s,p}$ and $D_{s,n}$ span numerous orders of magnitude depending on the electrochemical technique or specific material properties.[35] As such, this approach has an arbitrariness that is unsettling.

We can mimic the process of fixing constants to prior value estimates of θ (Table IV) in the literature, to assess the potential of this approach for addressing the lack of practical identifiability of some parameters. Fixing the three poorly identifiable parameters to prior values during the parameter estimation results in much poorer fits compared to the five-parameter Bayesian estimation (an increase in the objective function of 54% to 2840%, see Table V), which quantifies the potential limitations of fixing parameters to a constant.

2. Prior penalty term. This approach is described in the Maximum *A Posteriori* Estimation section. Priors explicitly account for the level of uncertainties in the prior estimates of the parameters and allows for more flexibility in the parameter estimation optimization compared to constants. If a prior parameter estimate has large uncertainty, then the identifiability issue is resolved while having nearly identical quality of fit to data as not using the prior at all. If the uncertainty in a prior parameter estimation is low, then the parameter estimation will appropriately bias its estimated parameter toward the prior. Due to the prior term being convex quadratic, the solution space for MAP estimation (Eq. 4) will be finitely bounded and tend to be easier to converge numerically than ML estimation (Eq. 3).

Figure 7 shows the pairwise posterior distributions obtained with MCMC under MAP estimation. The effective diffusivity $D_{s,n}$, which is identifiable with ML estimation, is likewise identifiable and its probability density is largely unaffected by the prior despite its peak being more than an order of magnitude away from the prior value. The PDFs of the other four practically unidentifiable parameters—$D_{s,p}$, D, k_p, and k_n—have a Gaussian PDF compared to the plateau in Figs. 4b–4e, which is a direct result of the prior term penalizing deviation from the mean. The normalized objective function from MAP estimation is 1.13, which is much lower than rigidly fixing parameters to constants.

3. Model reduction. Removing equations from the model is another method of alleviating practical unidentifiabilities. An added benefit of this method is that the simulation will run more quickly since fewer equations are required to be solved. Parameter

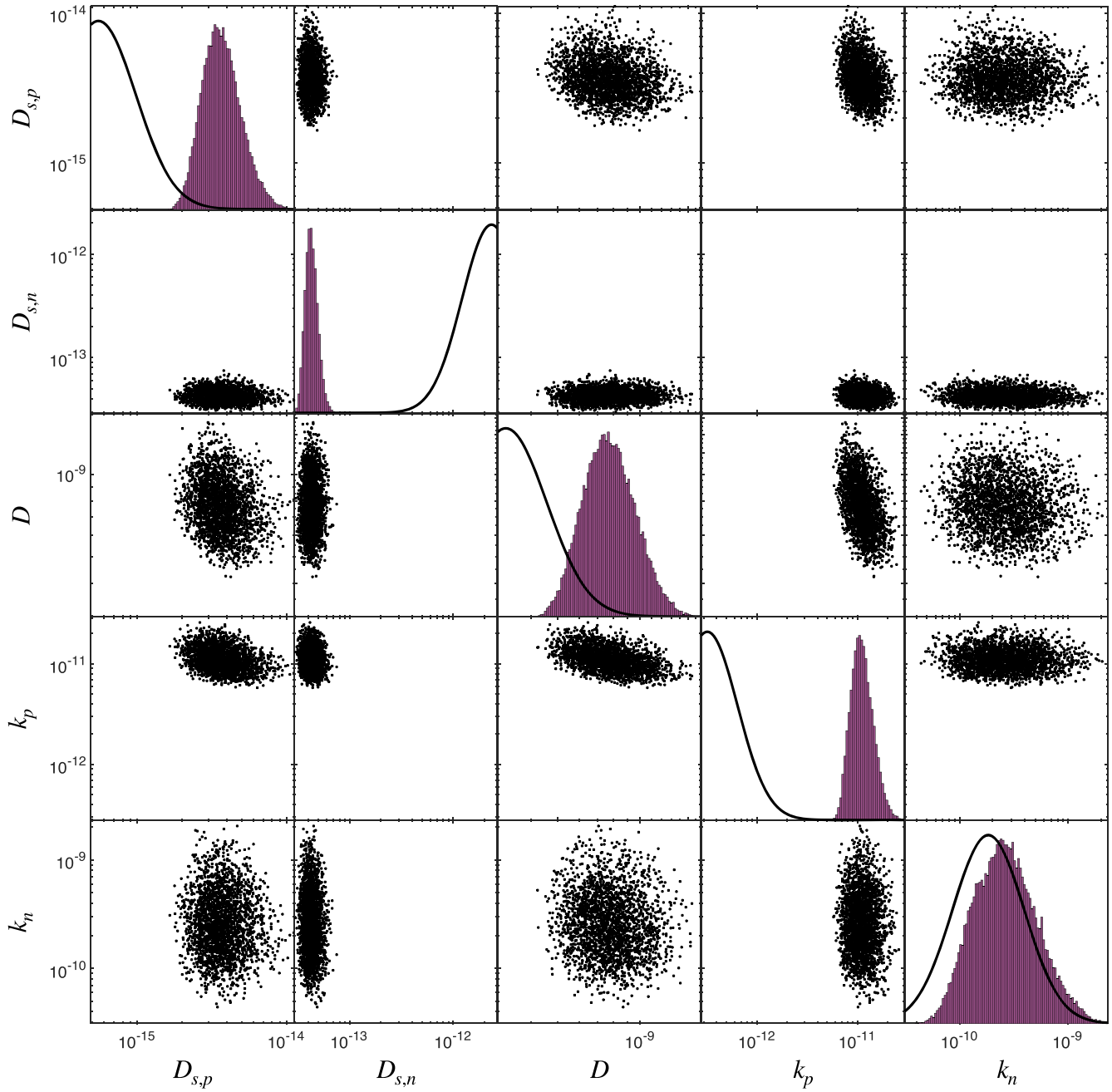

Figure 7. Pairwise posterior distributions determined by MCMC. Histograms of the variables are shown on the diagonal, and scatter plots of variable pairs are shown on the off-diagonal.

estimation will be quicker as well; similar to the method where parameters are constant, there are fewer degrees of freedom. In closed systems such as a battery simulation, it is important to carefully remove equations so the conversation equations are still maintained throughout the control volume.

4. Collecting more informative datasets. Identifiability problems can also be addressed by gathering more experimental data, such as by operating under very different conditions or collecting additional types of measurements. For lithium-ion batteries, nonlinearity identifiability analysis shows that the kinetic and transport parameters are not fully identifiable only using data from discharge curves under standard operations. For instance, discharge data for a reaction-limited cell cannot yield identifiable diffusion parameters. Equivalent circuit models (ECM) have widely been used with electrochemical impedance spectroscopy (EIS) to estimate diffusion coefficients in batteries[41,42] which fit impedance data over a range of frequencies. Short constant current pulses have been used to estimate rate constants in batteries in the absence of mass transfer limitations.[42,43] This methodology can additionally be used to design sets of experiments to produce data sets which probe a broad set of parameters of interest for optimal identifiability.

Conclusions

A nonlinear identifiability analysis was performed on the kinetic and transport coefficients of the pseudo-two-dimensional (P2D) model using a voltage discharge curve at constant discharge of C/10. Bayesian inference was performed on the set of parameters via the Metropolis-Hastings Markov chain Monte Carlo (MCMC) algorithm. Histograms produced from MCMC served as a preliminary screening of globally (un)identifiable parameters and were used to establish global 95% confidence intervals. The effective

solid diffusion coefficient was shown to be practically unidentifiable, whereas the other four are practically unidentifiable. Local identifiability of the unidentifiable parameters was further investigated visually using 2D and 3D confidence regions with contour plots and isosurfaces respectively. The confidence region of the locally unidentifiable parameters was shown to qualitatively depict resistances in series, effectively meaning only their summed resistance could be uniquely identified.

Various methods of dealing with identifiabilities, such as fixing parameters, adding priors, and removing equations in the model were discussed. Regressing on other experiments such as electrochemical impedance spectroscopy or current pulses can lead to a greater set of identifiable parameters. As the effective solid diffusion coefficient in the anode is the only identifiable model parameter in this system, this battery is in the diffusion-limited regime and requires orthogonal data sources to uniquely estimate the other parameters. It is important to contextualize the results in terms of the specific experimental data, set of modeling equations, and parameters used in the identifiability analysis. Different conditions will likely result in different conclusions—both of which can be accurate within the context of each specific problem.

Acknowledgments

This work was supported by the Toyota Research Institute through the D3BATT Center on Data-Driven-Design of Rechargeable Batteries. We thank Mike J. Bobman for discussions.

ORCID

Marc D. Berliner https://orcid.org/0000-0002-2511-1853
Supratim Das https://orcid.org/0000-0003-2138-9353
Richard D. Braatz https://orcid.org/0000-0003-4304-3484

References

1. M. Doyle, T. F. Fuller, and J. Newman, *J. Electrochem. Soc.*, **140**, 1526 (1993).
2. N. Jin, D. L. Danilov, P. M. J. Van den Hof, and M. C. F. Donkers, *International Journal of Energy Research*, **42**, 2417 (2018).
3. A. Jokar, B. Rajabloo, M. Désilets, and M. Lacroix, *J. Electrochem. Soc.*, **163**, A2876 (2016).
4. D. C. López, C. G. Wozny, A. Flores-Tlacuahuac, R. Vasquez-Medrano, and V. M. Zavala, *Industrial & Engineering Chemistry Research*, **55**, 3026 (2016).
5. J. C. Forman, S. J. Moura, J. L. Stein, and H. K. Fathy, *Journal of Power Sources*, **210**, 263 (2012).
6. A. Aitio, S. G. Marquis, P. Ascencio, and D. Howey, (2020), arXiv:2001.09890.
7. P. Kemper, S. E. Li, and D. Kum, *Journal of Power Sources*, **286**, 510 (2015).
8. V. Ramadesigan, K. Chen, N. A. Burns, V. Boovaragavan, R. D. Braatz, and V. R. Subramanian, *J. Electrochem. Soc.*, **158**, A1048 (2011).
9. J. Newman and W. Tiedemann, *AIChE J.*, **21**, 25 (1975).
10. T. F. Fuller, M. Doyle, and J. Newman, *J. Electrochem. Soc.*, **141**, 1 (1994).
11. T. F. Fuller, M. Doyle, and J. Newman, *J. Electrochem. Soc.*, **141**, 982 (1994).
12. W. Fang, O. J. Kwon, and C.-Y. Wang, *International Journal of Energy Research*, **34**, 107 (2010).
13. K. W. Baek, E. S. Hong, and S. W. Cha, *International Journal of Automotive Technology*, **16**, 309 (2015).
14. C. M. Doyle, "Design and Simulation of Lithium Rechargeable Batteries." *PhD thesis*, University of California, Berkeley (1995).
15. W. B. Gu and C. Y. Wang, *J. Electrochem. Soc.*, **147**, 2910 (2000).
16. M. Torchio, L. Magni, R. B. Gopaluni, R. D. Braatz, and D. M. Raimondo, *J. Electrochem. Soc.*, **163**, A1192 (2016).
17. J. V. Beck and K. J. Arnold, *Parameter Estimation in Engineering and Science* (Wiley, New York, NY) (1977).
18. R. Gunawan, M. Y. L. Jung, E. G. Seebauer, and R. D. Braatz, *AIChE J.*, **49**, 2114 (2003).
19. R. D. Braatz, R. C. Alkire, E. Seebauer, E. Rusli, R. Gunawan, T. O. Drews, X. Li, and Y. He, *Journal of Process Control*, **16**, 193 (2006).
20. Y.-H. Kao and M. C. Eisenberg, *Epidemics*, **25**, 89 (2018).
21. N. Dawson-Elli, S. B. Lee, M. Pathak, K. Mitra, and V. R. Subramanian, *J. Electrochem. Soc.*, **165**, A1 (2018).
22. S. Andradóttir, "A review of simulation optimization techniques." *Winter Simulation Conference* (IEEE, Piscataway, NJ) 1, 151 (1998).
23. A. Saltelli, M. Ratto, S. Tarantola, and F. Campolongo, *Chem. Rev.*, **105**, 2811 (2005).
24. J. R. Leis and M. A. Kramer, *Computers & Chemical Engineering*, **9**, 93 (1985).
25. R. Gunawan, D. L. Ma, M. Fujiwara, and R. D. Braatz, *International Journal of Modern Physics B*, **16**, 367 (2002).
26. E. Rusli, F. Xue, T. O. Drews, P. M. Vereecken, P. Andricacos, H. Deligianni, R. D. Braatz, and R. C. Alkire, *J. Electrochem. Soc.*, **154**, D584 (2007).
27. W. Q. Meeker and L. A. Escobar, *The American Statistician*, **49**, 48 (1995).
28. A. Raue, C. Kreutz, T. Maiwald, J. Bachmann, M. Schilling, U. Klingmüller, and J. Timmer, *Bioinformatics*, **25**, 1923 (2009).
29. N. Metropolis and S. Ulam, *Journal of the American Statistical Association*, **44**, 335 (1949).
30. S. Brooks, A. Gelman, G. Jones, and X.-L. Meng, *Handbook of Markov Chain Monte Carlo* (CRC Press, Boca Raton, Florida) (2011).
31. K. Binder, D. Heermann, L. Roelofs, A. J. Mallinckrodt, and S. McKay, *Comput. Phys.*, **7**, 156 (1993).
32. H. Haario, M. Laine, A. Mira, and E. Saksman, *Statistics and Computing*, **16**, 339 (2006).
33. S. Chib and E. Greenberg, *The American Statistician*, **49**, 327 (1995).
34. R. B. Smith and M. Z. Bazant, *J. Electrochem. Soc.*, **164**, E3291 (2017).
35. M. Hadigol, K. Maute, and A. Doostan, *Journal of Power Sources*, **300**, 507 (2015).
36. H. Xia, L. Lu, and G. Ceder, *Journal of Power Sources*, **159**, 1422 (2006).
37. K. Persson, Y. Hinuma, Y. S. Meng, A. Van der Ven, and G. Ceder, *Physical Review B*, **82**, 125416 (2010).
38. L. O. Valøen and J. N. Reimers, *J. Electrochem. Soc.*, **152**, A882 (2005).
39. A. Hess, Q. Roode-Gutzmer, C. Heubner, M. Schneider, A. Michaelis, M. Bobeth, and G. Cuniberti, *Journal of Power Sources*, **299**, 156 (2015).
40. Y. Chang, J. Jong, and G. T. Fey, *J. Electrochem. Soc.*, **147**, 2033 (2000).
41. C. R. Birkl and D. A. Howey, "Model identification and parameter estimation for LiFePO4 batteries." *IET Hybrid and Electric Vehicles Conference (HEVC)* (2013).
42. P. Kollmeyer, A. Hackl, and A. Emadi, "Li-ion battery model performance for automotive drive cycles with current pulse and EIS parameterization." *IEEE Transportation Electrification Conference and Expo(ITEC)* (IEEE, Piscataway, NJ) 486 (2017).
43. I. B. Goldberg and A. J. Bard, *The Journal of Physical Chemistry*, **78**, 290 (1974).